Journal of the European Ceramic Society 19 (1999) 591–599

PII: S0955-2219(98)00231-3
0955-2219/99/$—see front matter

Crack Closure Stresses in Fiber Reinforced Brittle Matrix Composites

H. Xu and C. P. Ostertag*

CEE Department, University of California, Berkeley, CA 94720, USA

(Received 24 June 1998; accepted 20 September 1998)

Abstract

The fracture toughness of an alumina ceramic and a continuous SiC fiber reinforced alumina composite processed by pressureless sintering was studied in situ in a Scanning Electron Microscope (SEM). The applied stress intensity factor was obtained as a function of both applied load and crack extension. Closure stresses across crack surfaces imposed by grain-bridging and fiber-bridging, and hence fracture resistance from bridging were studied by both stress intensity factor and J-integral considerations. Theoretical calculations agree with experimental results. An average fracture resistance of $\approx 40\ J\,m^{-2}$ *per fiber and a corresponding toughness of* $\approx 1{\cdot}6\ MPam^{1/2}$ *per fiber was obtained for fiber elastic bridging before fiber failure. Fiber-matrix interfacial properties were examined and a technique for evaluating interfacial frictional shear stress was developed.* © *1999 Published by Elsevier Science Limited. All rights reserved*

Keywords: fracture, Al_2O_3, fibers, SiC, interfaces.

1 Introduction

Fracture toughness as high as $40\,MPam^{1/2}$ and $50\,MPam^{1/2}$ have been achieved in continuous fiber reinforced ceramic composites.[1,2] In these materials, a major portion of the toughness is attributable to the work required to elastically elongate the bridging fibers and to frictionally pull the broken fibers out of the matrix. A complete understanding of reinforcement-toughening mechanisms would include fiber-crack interactions and the relative importance of various toughening mechanisms, such as fiber elastic bridging, broken fiber pullout and matrix grain bridging. Micromechanics studies of the toughening process, which are not yet available, are the key to achieving such an understanding. Direct experimental examination of the relative importance of various toughening mechanisms and the interaction between matrix cracks and reinforcing fibers are therefore valuable.

Ceramic matrix composites are currently densified by hot-pressing, chemical vapor, or reaction-bonding. Commercialization of any of these processes is hindered by technological and economic difficulties. The fiber reinforced composites in this study are pressureless sintered, a potential alternative process for fabricating near-net-shape composites. A composite processed by pressureless sintering may have different mechanical properties than those processed by other techniques, since the state of residual stresses and the interfacial properties may be different. Therefore, it is important to examine: how pressureless sintering influences mechanical properties; how the interfacial properties differ in a pressureless sintered composite from those of a hot-pressed composites; how the mechanical properties (i.e. fracture strength) of fibers change in pressureless sintering and how this affects the interactions of matrix cracks with fibers; and if mechanical properties can be improved by pressureless sintering.

In the pressureless sintered fiber reinforced composite under investigation, both fiber-bridging and matrix grain-bridging are operative. Grain-localized bridging as a toughening mechanisms in alumina was confirmed directly with in-situ observations of, crack propagation by optical microscopy,[3] and scanning electron microscopy.[4,5] It was observed that individual bridging grains interlock between the crack planes behind the advancing crack tip, sliding frictionally against matrix grains during crack opening. It is this frictional sliding that consumes energy and results in a rising resistance curve. The combination of grain-and fiber-bridging enhances the crack growth resistance even further by exerting additional closure stresses on the crack

*To whom correspondence should be addressed

walls. These closure stresses shield the crack tip from the applied load. In order for an existing crack to extend, a higher stress needs to be applied. Crack closure stresses associated with fiber- and grain-bridging are obtained from crack profiles measured at high magnification inside the scanning electron microscope.

2 Experimental Procedure

2.1 Specimen preparation

Both composite samples and monolithic samples were prepared by pressureless sintering. Several sheets of tape-casted Al_2O_3 green tapes stacked together to form a square specimen with fibers embedded between the tapes. The green thickness was approximately 4 mm. The fibers were SCS-2 SiC fibers (Textron Specialty Materials, MA), with a total diameter of 140 μm including a 33 μm carbon core and a carbon-rich surface coating of 2 μm. These fibers were coated with a layer of gold of 60 mm thickness before they were embedded in the tapes to reduce the chemical reaction between SiC and Al_2O_3.[6] The square specimens were then cold-pressed uniaxially at 13 MPa. After the binder burnout at 500°C for 8 h, the specimens were pressureless sintered at 1600°C for 2 h in air. The grain size of these specimens ranged from 2 to 15 mm, with an average grain size of 8 μm. The density was 3·7 g cm^{-3}, 93% of the theoretical density. In this study six fibers were embedded in each specimen, with two fibers in each plane along the specimen thickness. Monolithic Al_2O_3 samples without fiber reinforcement were processed in the same way to serve as control specimens.

The sintered square specimens (edge length approx. 18 mm) were ground to a thickness of 1·5–2 mm, and polished with diamond paste to a 6 μm finish on the surface for crack length measurements. Loading holes were drilled and notches sawed to form compact tension specimens to ASTM specifications. The notch was sawed through the first plane of fibers, so that only the second plane of fibers served as bridging ligaments during testing. The first and the third planes of fibers fulfilled the symmetry requirements during densification. The notch was cut at an angle of 45° to the specimen surface in a half-chevron geometry to enhance the stability in the initial crack extension. Accordingly, the notch tip extended 1 mm further on the unpolished surface compared to the polished surface. A Vickers indentation, contact load 50 N was placed 200 μm ahead of the notch tip on the polished surface, which left a starter crack. The specimen was then precracked in a preliminary load cycle to create a crack from the notch tip going through the indent. After a crack length of approximately 1300 μm was propagated, the half chevron wedge including the indent was carefully sawed away, leaving a notch of constant thickness and a precrack of 300 μm from the notch tip. The crack tip is several hundred microns away from the second row of fibers which will serve as bridging ligaments in subsequent *in-situ* crack propagation studies inside the SEM.

2.2 SEM measurements of crack propagation

The precracked specimens were coated with Au–Pd to a thickness of 25 mm. A custom designed loading device was used to apply a mechanical load to compact tension specimens as crack growth was observed in the SEM. After the specimens were placed in the device and loaded inside the SEM to propagate the crack, events occurring at the bridging sites were monitored and recorded on film and video tapes. Both crack tip propagation and crack wake grain- and fiber-bridging were observed and video taped. This was done along the crack paths for crack opening displacement (COD) measurements. The COD measurements were made only in well-behaved regions, i.e. at grain facets oriented normal to the load axis and located away from any secondary cracking around bridging sites. The cracks were rendered highly visible in the secondary electron mode by edge charging. This charging limited the absolute resolution of surface-surface separation to about 70 nm, although relative measurements could be made to better than 30 nm. Typical COD values were in the range of 50–100 nm which are too small to be measured by optical techniques. SEM techniques are required for accurate measurements.

3 Results

3.1 Observation of bridging sites

In-situ SEM observation revealed that both grain-bridging and fiber-bridging were operative along the crack paths. Crack propagation occurred in a discontinuous fashion and the fracture mode was predominantly intergranular. For the monolithic specimens, grain-bridging occurred throughout the entire crack path. The final crack lengths before failure were typically 600 mm with maximum CODs in the range of 0·4 μm. In the fiber reinforced samples where both grain-bridging and fiber-bridging were operative, much longer cracks with 2 mm length and maximum CODs of 1·4 μm were stable under higher applied load, indicating the effectiveness of fiber-bridging. SEM pictures of grain-bridging and fiber-bridging are shown in Fig. 1(a) and (b), respectively.

3.2 *In-situ* measurement of crack-opening displacements

Crack opening displacements were measured for both monolithic and fiber-reinforced specimens. The crack profile when the stress-intensity factor, K_a, was $4\,\mathrm{MPam}^{1/2}$ for a monolithic specimen is shown in Fig. 2(a). The crack profile of a specimen with two bridging fibers is shown in Fig. 2(b) for a stress intensity factor of $7\,\mathrm{MPam}^{1/2}$. The positions of the two bridging fibers are indicated. The COD values, together with the fiber-matrix interfacial frictional shear stress, τ, enable the evaluation of the bridging force in each individual fiber, as will be shown later.

3.3 Applied stress intensity factor

The applied stress intensity factor is the driving force for crack propagation, while the toughness of the material is the resistance to crack propagation. The resistance to crack propagation results from the intrinsic toughness, T_o, of the material (related to the atomic bond strength), and the toughness increase from crack closure forces due to grain-bridging, T_g. and fiber-bridging. T_f. At equilibrium

$$K_a = T_o + T_g + T_f \tag{1}$$

For monolithic specimens, the third contribution T_f is zero. The applied stress intensity factor, K_a, is never felt at the crack tip in the composites due to shielding by grain- and fiber-bridging.

For the compact tension test in this study, K_a, can be readily calculated by,

$$K_a = (F/tw^{1/2})\,Y(a/w) \tag{2}$$

where F is the applied load recorded during crack propagation, t and w are the specimen dimensions and a is the crack length measured from the center of the loading holes. The crack geometry function $Y(a/w)$ is given by:[7]

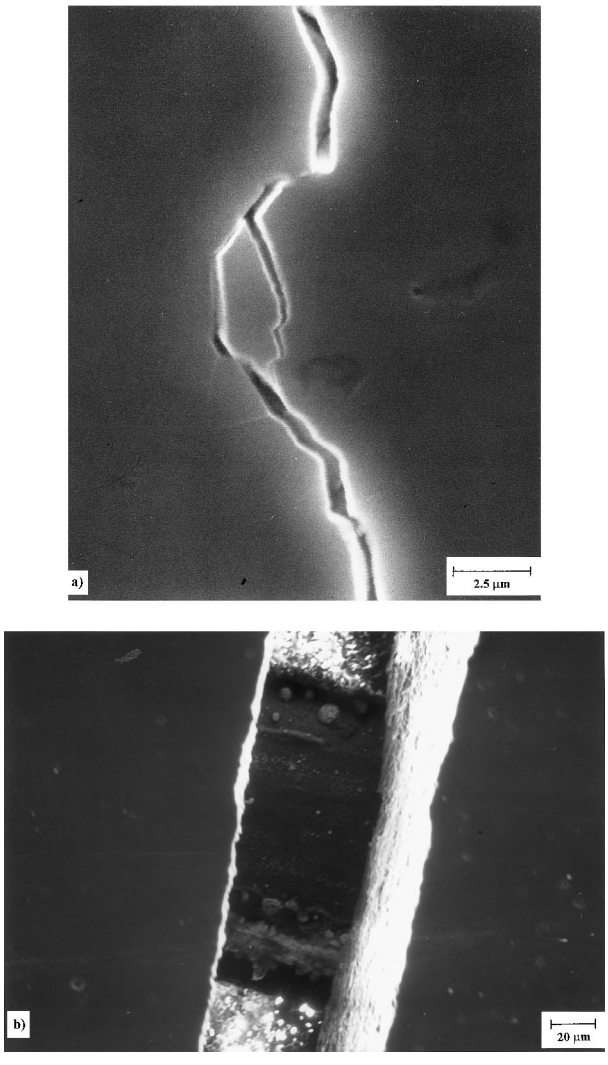

Fig. 1. SEM micrographs of (a) grain bridging at crack interface behind the crack tip; (b) SiC fiber bridging crack faces.

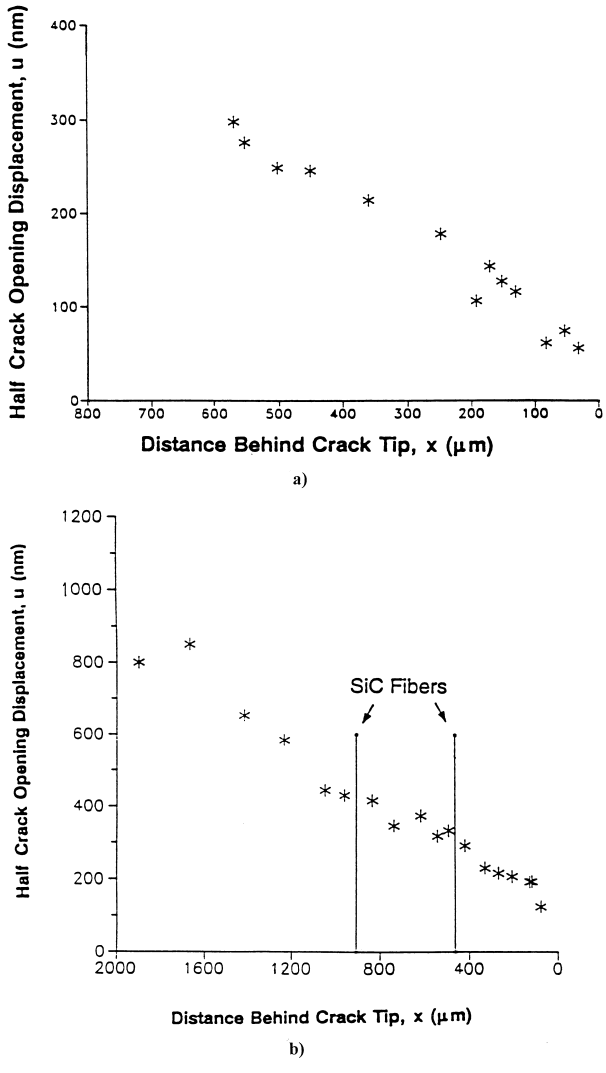

Fig. 2. Measured crack opening displacements (COD) at crack interfaces: (a) in alumina, (b) in a SiC fiber reinforced alumina compact tension specimen.

$$Y(a/w) = (2 + a/w)/(1 - a/w)^{3/2} [0{\cdot}886 + 4{\cdot}64(a/w) - 13{\cdot}32(a/w)^2 + 14{\cdot}72(a/w)^3 - 5{\cdot}6(a/w)^4] \quad (3)$$

For both the monolithic specimens and fiber reinforced specimens, K_a was calculated as a function of the applied load and the crack extension. For the monolithic specimens, K_a, reached a maximum value (after which the specimen broke) of 4·3 MPam$^{1/2}$. With two bridging fibers, a maximum K_a of 7·4 MPam$^{1/2}$ was obtained. The increase in toughness with crack extension for one of the fiber reinforced composites is shown in Fig. 3.

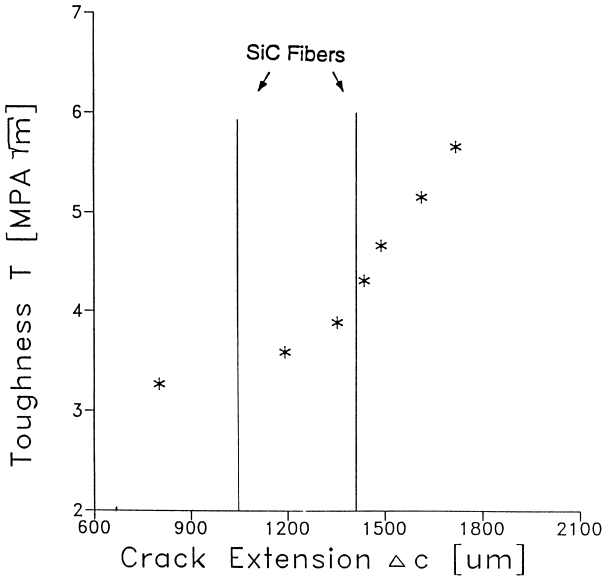

Fig. 3. Measured toughness as a function of crack extension for a fiber-reinforced alumina specimen with two fibers in the bridging zone.

4 Analysis and Discussion

Consider a crack that moves in the matrix towards a fiber. Fiber debonding can occur either ahead of the crack front before the crack reaches the fiber or after the crack passes the fiber, depending on the elastic modulus difference between the matrix and the fiber. If the difference is large enough, fiber-matrix debonding may occur before the crack reaches the fiber due to strain mismatch. On the other hand, if the elastic moduli are similar, as in this study ($E_m = 400$ GPa, $E_f = 410$ GPa), strain mismatch is small and fiber-matrix debonding occurs only after the crack meets the fiber and is deflected along the interface or around the fibers. Subsequent increases in applied load drive the crack past the fiber, with an increase in debonding length L_d, and an increase in COD at the fiber position. Accordingly, the tensile strain in the fiber is enhanced which increases the bridging stress across the crack walls yielding the *R*-curve behavior. The debonded part of the fiber is partially pulled out of the matrix. Fiber failure usually occurs away from the crack plane due to a distribution of strength in fibers. The broken fiber is then pulled out of the matrix upon further opening of the crack. The term 'pullout' has been used in literature to describe only the toughening process after fiber failure when the broken fiber is being pulled out of the matrix. The term 'bridging' has been used to describe the toughening process before fiber failure. Strictly speaking, both bridging and pullout occur throughout the entire process of toughening, both before and after fiber failure. To avoid confusion the term 'elastic bridging' will be used in this paper to describe toughening before fiber failure, and frictional pullout to describe toughening after fiber failure. Usually the fiber pullout length, L_p, is much larger than the maximum COD before fiber failure, and the crack resistance as a result of frictional pullout may be comparable to or larger than that of elastic bridging. For composites reinforced uniformly with a substantial volume percent (i.e. 30%) of fibers, elastic bridging and frictional pullout occur simultaneously during crack propagation. Therefore, their contributions to crack resistance can not be measured separately. For specimens in this study only two fibers are bridging the crack during stable crack propagation. When one fiber failed, the other fiber and the specimen broke immediately due to the sudden increase in stress. Therefore, measurement of contribution from fiber frictional pullout after fiber failure was not taken. This allowed the measurement of toughness increase from elastic bridging alone, the contribution from pullout after fiber failure was not a factor.

The debonded part of the fiber that provides the closure stress is elongated elastically and therefore in tension. At the crack plane, the tensile stress in the fiber as a function of half crack opening u, $\sigma_f(u)$, acts to pull the fiber out of the matrix. This is opposed by the frictional stress at the fiber-matrix interface:

$$\sigma_f(u)\pi R^2 = \tau 2\pi R L_d \quad (4)$$

where R is the fiber radius, and r is the frictional shear stress between the debonded fiber of length L_d and the matrix. The tensile stress in the fibers may also be expressed as a function of the crack opening displacement, u, (see Appendix A):

$$\sigma_f(u) = (4E_f \tau u/R)^{1/2} \quad (5)$$

where E_f is the Young's modulus of the fiber.

4.1 Fracture strength of fibers in matrix

The fracture strength of the as-received SCS-2 SiC fibers was measured to be 4 GPa at a gauge length of 20 mm. When they are embedded in the $A1_2O_3$ matrix and sintered in air, the fracture strength of the fibers degrades due to fiber grain growth and chemical reactions. Fiber degradation due to chemical reaction was reduced in this study by a protective gold coating applied to the fibers before embedding them in the matrix.

If we consider the fiber fracture strength to be single-valued (Weibull modulus $m=\infty$), fiber failure will occur between the crack faces where the tensile stress in the fiber is a maximum. However, fibers exhibit a strength distribution due to the presence of flaws and fiber failure usually occurs away from the crack plane, resulting in fiber pullout. The fiber pullout length, L_p, corresponds to the distance from the crack plane, Z_f, at which fiber failure occurs. The tensile stress in the fiber at failure at a distance Z_f, is the fracture strength of the *in-situ* fiber, S. The fracture strength of these embedded fibers can be evaluated for each individual fiber by measuring the mirror radius, a_m, on the fiber fracture surface, as demonstrated by Thouless *et al.*[8]

$$S = 3{\cdot}5K_f/a_m^{1/2} \tag{6}$$

where K_f is the fiber fracture toughness which is approximately 2 $MPam^{1/2}$.[8] The fracture strength for each individual fiber can thus be calculated and an average value can be obtained. In this study $S=2$ GPa was obtained for the in-situ fiber strength after the sintering process.

4.2 Interfacial frictional shear stress

The interfacial shear stress τ can be obtained as shown in Appendix B:

$$\tau = RE_f u_o/4L_p^2[1-(1-2SL_p/E_f u_o)^{1/2}]^2 \tag{7}$$

where u_o is the half COD at the fiber position when fiber failure occurs. In this equation S can be evaluated as described in Section 4.1, u_o and L_p can be measured experimentally for each fiber, and E_f and R are known constants. Using this equation an average value of $\tau=1{\cdot}3$ GPa was obtained for specimens in this study.

An interfacial frictional shear stress of 1·3 GPa is large compared to values of generally <100 MPa reported in the literature.[9–14] When the thermal expansion coefficient of the matrix is larger than that of the fibers as in this study, the fibers are in radial compression when the specimen is cooled from the sintering temperature. In this case τ can be expressed by

$$\tau = \sigma_R \mu \tag{8}$$

where σ_R is the residual stress at the interface in the fiber radial direction, and μ is the frictional coefficient at the debonded interface. There are three possible reasons for the high value of τ in the specimens of this study. First, the large difference in thermal expansion coefficients between the SiC fiber and the alumina matrix $(\alpha_m-\alpha_f > 4\times10^{-6}/^\circ C)$ results in a high value of σ_R when the specimen is cooled from the sintering temperature of 1600°C to room temperature. Assuming the residual stress above 1200°C relaxes due to creep, an estimate of the residual stress at room-temperature results in $\sigma_R = E\Delta\alpha\Delta T \approx$ (400 GPa)$(4\times10^{-6}/^\circ C)=1{\cdot}9$ GPa. The composite materials reported in literature, with glass matrices in most cases, have much smaller thermal mismatches between the matrices and fibers.[9–14] The second reason for the high frictional stress may by associated with the pressureless sintering process. Most fiber reinforced composites are processed by hot-pressing, while the specimens in this study are processed by pressureless sintering. In hot-pressing the residual stresses result mainly from thermal expansion mismatch. In sintering the matrix shrinks 30 to 40 vol% while the fibers, being fully dense, do not shrink at all. This gives rise to an additional compressive stress at the interface perpendicular to the fibers which do not relax completely by creep.[15] Thirdly, a thin reaction layer between the fibers and the matrix was found after sintering. This may increase the roughness of the interface after debonding, increasing the frictional coefficient, μ, between the sliding fiber and the matrix. Therefore, the higher value of τ may be associated with higher values of both σ_R and μ. Higher values of τ are of practical importance in achieving high short-crack toughness.[16]

A number of techniques have been proposed to measure the interfacial shear stress, τ. These techniques may not be well suited for the fiber reinforced composites in this study with high interfacial frictional shear stress. Fiber cracking can occur in push-in tests when the load is high.[17] The slice-compression technique[11,14] is not effective when the Young's modulus of fibers is close to that of the matrix, as in this study. Furthermore, various techniques often reveal very different results (i.e. the value of τ by the slice-compression technique was an order of magnitude smaller compared with the fiber pull-out technique for the same composite[11]). The technique for measuring τ described in this section is believed to be fairly dependable compared to other techniques, especially when τ is large.

4.3 Closure stresses associated with grain-and fiber-bridging

4.3.1 Grain-bridging

Grain localized bridging at the crack interface behind the advancing crack tip increases the crack growth resistance of the material. When the crack opens, grain pullout occurs and the fraction at the sliding matrix-grain interface contributes to the resistance. Grain-bridging, exerts a closure stress across the crack faces. The closure stress $\sigma(u)$ as a function of u can be expressed as[18]

$$\sigma(u) = \sigma_m(1 - u/u^*) \tag{9}$$

where σ_m is the maximum closure stress which occurs at the crack tip ($u = O$), and u^* is the half COD at the end of a saturated bridging zone.

When steady state is reached, the bridging zone is saturated. When the increase in K_a with crack length is faster than the increase in toughness, T, the specimen fails when the crack length reaches a critical value. In this case the bridging zone is not saturated, and the maximum crack opening before failure, $2U_b$, is less than the steady state opening $2u^*$. The crack resistance can be calculated using eqn (9) and the J-integral:

$$\begin{aligned} R_g &= 2\int_0^{u_b} \sigma_m(1 - u/u^*)\mathrm{d}u \\ &= 2\sigma_m u_b(1 - u_b/2u^*) \end{aligned} \tag{10a}$$

When steady, state is reached, $u_b = u^*$, therefore

$$R_g^* = \sigma_m u^* \tag{10b}$$

For the Al_2O_3 compact tension specimens in this study, experimental measurements gave $u_b \approx 0{\cdot}22\,\mu$m. The steady state half COD, u^*, is a fraction of the grain size, L. In this study, L was $8\,\mu$m. Taking literature values for $\sigma_m = 79$ MPa[4] and 'bridging rupture' strain ε_1, equal to 0·1[18] we obtain $u^* = 0{\cdot}4\,\mu$m ($u^* = \varepsilon_1 L/2$). Inserting these parameters into eqn (10a) results in $R_g = 22$ J m^{-2}. For, Al_2O_3 with its intrinsic resistance R_o of 17 J m^{-2},[19] the total resistance $R = R_o + R_g$ is 39 J m^{-2}, corresponding to a toughness value $T = (E'R)^{1/2}$ of 4·2 MPam$^{1/2}$. The calculated toughness value agrees well with the experimental measurement of $K_a = 4{\cdot}3$ MPam$^{1/2}$. Therefore, the grain bridging model gives a toughness value consistent with that obtained from the stress-intensity approach.

When steady state is reached, inserting the parameters above into eqn (10b) results in $R_g^* = 28$ J m^{-2}, yielding a total crack resistance R^* of 45 J m^{-2}, and a corresponding maximum toughness T^* of 4·4 MPam$^{1/2}$.

4.4 Grain-bridging plus fiber-bridging

For a material with both grain- and fiber-bridging, the toughness and the crack resistance have three major contributions: the intrinsic fracture toughness of the matrix (T_o); grain bridging and pullout (T_g); and fiber bridging and pullout (T_f). Thus:

$$T = T_0 + T_g + T_f \tag{11a}$$

or

$$R = R_o + R_g + R_f \tag{11b}$$

Where $R_o = T_o^2/E'LR = T^2/E'$, and $R_f = R_r^e$ (elastic bridging)$+R_f^p$ (broken-fiber pullout), $E' = E/(1 - \nu^2)$. The specimens in this study with two bridging fibers only the resistance due to elastic fiber-bridging was measured and calculated, R_f^p was not included. This allowed direct evaluation of the effects of elastic fiber-bridging.

For a composite with a substantial volume fraction of reinforcing fibers uniformly aligned along the crack plane, the bridging effect can be represented by a continuous closure stress, p, over the fiber bridging zone of length x_f. The crack growth resistance can be calculated by the J-integral:

$$R_f = 2\int_0^{uf} P(u)\mathrm{d}u \tag{12a}$$

where u_f is the crack opening at the end of the fiber bridging zone. When $u = u(x)$ is known as a function of x(x is the coordinate along the crack length, with the origin at the crack tip), eqn (12a) can be written as:

$$R_f = 2\int_0^{xf} \sigma(x)(\mathrm{d}u/\mathrm{d}x)\mathrm{d}x \tag{12b}$$

where $\sigma(x)$ is the closure stress, $\sigma = p$. Here p is expressed as a function of u, while σ is expressed as a function of x, i.e. $\sigma(x) = p(u(x))$. The resistance can hence be calculated when the closure stress is known as a function of COD or as a function of crack length. Usually, the closure stress is known as a function of x, since u is too small to be measured by conventional techniques. But in this study, due to the advantage of the SEM *in-situ* measurements, the closure stress can be obtained both as a function of x and u.

Alternatively, the toughness can be calculated using the Barenblatt relation.[20] In the small bridging zone limit, where $x_f \ll c$, the Barenblatt equation evaluates the toughness increase from the closure stress as:

$$T_f = (2/\Pi)^{1/2}\int_0^{xf} [\sigma(x)/x^{1/2}]\mathrm{d}x \tag{13}$$

The results of eqns (12) and (13) should agree with each other to be consistent.

When there are only a few fibers bridging a narrow region of the crack, a continuous closure stress can be approximated over the narrow bridging region, $x_1 \leq x \leq x_2$. If the fibers are far apart from each other, it is more appropriate to use point forces instead of a continuous stress. In this study, the two bridging fibers were very close to each other in a narrow bridging zone of 500 μm. Accordingly, the use of a continuous closure stress within the narrow bridging zone, $x_1 \leq x \leq x_2$, is appropriate and the crack resistance due to fiber-bridging is:

$$R_f = 2\int_{u1}^{u2} p(u)\mathrm{d}u = 2\int_{x1}^{x2} \sigma(x)(\mathrm{d}u/\mathrm{d}x)\mathrm{d}x \qquad (14)$$

where $2u_1$, and $2u_2$ are the CODs at x_1 and x_2, respectively. Both u and x are measured experimentally.

Alternatively, inserting this narrow bridging zone into the Barenblatt equation gives:

$$T_\mathrm{f} = (2/\pi)^{1/2}\int_{x1}^{x2} [\sigma(x)/x^{1/2}]\mathrm{d}x \qquad (15)$$

For specimens with fiber bridging, a stable crack of $\approx$2 mm length was obtained with a maximum u of 0·7 μm. Since this COD exceeds $u^* = 0{\cdot}4\,\mu$m, steady-state grain-bridging was achieved. As shown in Fig. 3(a) and (b), the crack profile differs for fiber reinforced specimens compared to the monolithic samples due to the closure stress from fiber-bridging. Since the deviation of the crack profile from linear is slight, the result for monolithic Al_2O_3 obtained from eqn (10b) was used to represent the grain-bridging contribution here. Since steady-state was reached, $R_\mathrm{g} = R_\mathrm{g}^* = 28\ \mathrm{J\,m^{-2}}$.

The maximum tensile stress in each bridging fiber before failure was calculated from eqn (5) using the measured value of COD and the calculated value of τ. The average value of σ_f was 3·2 GPa. This value exceeds the fiber fracture strength S because σ_f corresponds to the fiber stress at the crack plane with maximum tensile strain, while the fiber failure occurred at a weak point of the fiber away from the crack plane. The tensile force in the fibers at the crack plane divided by the bridging zone area results in the closure stress within the bridging zone. The closure stress thus obtained is $p = \sigma = 197$ MPa. Using this value and the measured COD values, eqn (14) results in $R_\mathrm{f} = 76\ \mathrm{J\,m^{-2}}$ and $R = R_\mathrm{o} + R_\mathrm{g}^* + R_\mathrm{f} = 121\ \mathrm{J\,m^{-2}}$. Correspondingly, a total toughness $T = (RE')^{1/2}$ of 7·3 $\mathrm{MPam^{1/2}}$ was obtained.

Alternatively, with the measured values of x_1 and x_2 and the calculated closure stress of $\sigma = 197$ MPa, eqn (15) results in $T_\mathrm{f} = 3{\cdot}1\ \mathrm{MPam^{1/2}}$ and $T = T_\mathrm{o} + T_\mathrm{g}^* + T_\mathrm{f}$ or 7·5 $\mathrm{MPam^{1/2}}$. Both results are consistent with the experimental value of the applied stress intensity factor, $K_\mathrm{a} = 7{\cdot}4\ \mathrm{MPam^{1/2}}$.

An increase in crack growth resistance of 76 $\mathrm{J\,m^{-2}}$ and a corresponding fracture toughness increase of 3·2 $\mathrm{MPam^{1/2}}$ from the elastic bridging of two fibers is remarkable, compared to an increase in fracture toughness of only 0·2 $\mathrm{MPam^{1/2}}$ by one bridging fiber in a glass matrix.[12–14] This increase in fracture toughness in our study is attributed to the large interfacial fictional stress, τ compared with those in glass specimens, where τ is so low that the embedded fiber can be pulled out of the matrix completely without breaking. The accompanying crack resistance is practically unusable in industrial applications since the crack opening is too large (in the order of the length of the embedded fiber). Therefore. optimum values of τ, not minimum values of τ, need to be investigated to achieve maximum crack resistance within the maximum practical COD. To achieve a steep rising R-curve, this work based on elastic bridging suggests the need to increase τ in continuous fiber reinforced composites with low τ values.

The final debond length, L_fd, of fibers before failure can be calculated from Appendix B

$$L_\mathrm{fd} = 2L_\mathrm{p}/[1 - (1 - 2\sigma_\mathrm{f}L_\mathrm{p}/E_\mathrm{f}u)^{1/2}] \qquad (16)$$

Numerical calculations using the measured values of L_p, σ_f and u result in $L_\mathrm{fd} = 90\ \mu$m on average for the specimens studied. This debond length is small compared to the fiber diameter due to the large value of τ.

5 Summary

- Alumina specimens reinforced with continuous SiC fibers were processed by pressureless sintering and exhibit both grain- and fiber-bridging.
- Crack propagation and crack profile measurements were performed in situ inside the SEM. The crack profile measurements provide information on crack tip shielding due to grain- and fiber-bridging.
- Crack resistance and fracture toughness as a function of crack extension were computed by both stress intensity considerations and the J-integral, together with the applied stress intensity factor. The results were shown to be self-consistent.
- The fracture strength of fibers in the matrix were evaluated. A technique for measuring the

fiber-matrix interfacial frictional stress τ was developed. The importance of the interfacial frictional stress was discussed.

- A crack resistance of $\approx 40\ \mathrm{J\,m^{-2}}$ per fiber due to elastic fiber-bridging was obtained for the fiber reinforced composites.

References

1. Zok, F., Sbaizero, O., Horn, C. L. and Evans, A. G., Mode I fracture resistance of a laminated fiber-reinforced ceramic. *J. Am. Ceram. Soc.*, 1991, **74**(1), 187–193.
2. Nair, S. V., Gwo, T. J., Narbut, N. M. and Kohl, L.G., Mechanical behavior of a continuous SiC fiber reinforced RBSN-matrix composite. *J. Am. Ceram. Soc.*, 1991, **74**(10), 2551–2558.
3. Swanson, P. J., Fairbanks, C. J., Lawn, B. R., Mai, Y. W. and Hockey., B. J., Crack-interface grain bridging as a fracture resistance mechanism in ceramics: I. Experimental study on alumina. *J. Am. Ceram. Soc.*, 1987, **70**(4), 279–289.
4. Rodel, J., Kelly, J. F. and Lawn, B. R., In situ measurements of bridging crack interfaces in the scanning electron microscope. *J. Am. Ceram. Soc.*, 1990, **73**(11), 3313–3318.
5. Frei, H. and Grathwohl, G., New test method for engineering ceramics—in situ microscopy investigation. *Ceram. Forum Int.*, 1991, **68**, 27–33.
6. Ostertag, C. P., Chemical reaction between Al_2O_3 and SiC at the fiber/matrix interface. Unpublished work.
7. ASTM designation E 399, standard test method for plane-strain fracture toughness of metallic materials. In *ASTM Standards*, Part 10. American Society for Testing and Materials, Philadelphia, PA, 1981.
8. Thouless, M. D., Sbaizero, O., Sig, L. S. and Evans, A. G., Effect of interface mechanical properties on pullout of a SiC fiber reinforced lithium aluminum silicate glass ceramic. *J. Am. Ceram. Soc.*, 1989, **72**(4), 525–532.
9. Weihs, T. P. and Nix, W. D., Experimental examination of the push-down technique for measurina the sliding resistance of silicon carbide fibers in a ceramic matrix. *J. Am. Ceram. Soc.*, 1991, **74**(3), 524–534.
10. Kerans, R. K., Hay, R. S. and Pagano, N. J., The role of the fiber-matrix interface in ceramic composites. *Ceramic Bulletin*, 1989, **68**(2), 548–553.
11. Shafry, N. Brandon, D. G. and Terasaki, M., Interfacial friction and debond strength of aligned ceramic matrix composites. In *Euro-Ceramics, Vol. 13, Engineering Ceramics*, eds G. de With, R. A. Terpstra and M. Metselear, Elsevier Applied Science, London, 1989, 453–464.
12. Coyle, T. W., Fuller Jr, E. F. and Swanson, P., Fracture mechanics characterization of crack/fiber interactions in ceramic matrix composites. *Ceramic. Engr. and Sci. Proc.*, 1987, **8**(7–8), 258–264.
13. Coyle, T. W., Palamides, T. R., Freiman, S. W., Fuller, Jr, E. R. and Deshmukh, U. V., Crack-fiber interactions in ceramic matrix composites. Proceedings of the 1987 Yortheast Regional meeting of TMS, High Temperature Structural Composites: Synthesis, Characterization, and Properties. HoBoken, NJ, 1987, p. 1458–1464.
14. Butler. L., Ph.D. thesis, Mechanical properties of fibre reinforced glass matrix composites. Lehigh University, Bethlehem, PA. 1993.
15. Ostertag, C. P., Drescher-Krasicka, E., Novel residual stress measurement techniques in fiber reinforced composites. *J Mat. Sci.*, in press for publication.
16. Xu, H., Ostertag, C. P., Braun, L. M. and Lloyd, I., Short crack mechanical properties and failure mechanisms of Si_3N_4 matrix SiC fiber composites. *J. Am. Ceram. Soc.*, 1994, **77**(7), 1889–1896.
17. Brun, M. K. and Singh, R. N., Effect of thermal expansion mismatch and fiber coating on the fiber/matrix interfacial shear stress in ceramic matrix composites. *Ad. Ceram. Mat.*, 1988, **3**(5), 506–509.
18. Bennison, S. J. and Lawn, B. R., Role of interfacial grain-bridging sliding friction in the crack-resistance and strength properties of nontransforming ceramics. *Acta Metall.*, 1989, **37**(10), 2659–2671.
19. Chantikul, P., Bennison, S. J. and Lawn, B. R., Role of grain size in the strength and R-curve properties of alumina. *J. Am. Ceram. Soc.*, 1990, **73**(8), 2419–2427.
20. Barenblatt, G. I., The mathematical theory of equilibrium cracks in brittle fracture. *Adv. Appl. Mechan.*, 1962, **7**, 55–129.

Appendix A

From eqn (4) in the text, it can be obtained that:

$$\sigma_f(u) = L_d\tau/R \tag{A1}$$

Taking Z as the coordinate axis in the direction parallel to the fiber with the origin at the crack plane, the tensile stress, $\sigma(Z)$, in the fiber at an arbitrary position, Z, within the debonded region can be obtained. Since

$$\sigma(z)\pi R^2 = 2\pi R\tau(L_d - Z) \tag{A2}$$

therefore

$$\sigma(Z) = 2\tau(L_d - Z)/R \tag{A3}$$

Then the tensile strain in the fiber at position Z is

$$\varepsilon_z = \sigma(z)/E_f = 2\tau(L_d - z)/RE_f \tag{A4}$$

The half crack opening displacement, u, can thus be calculated using eqn (A4) as:

$$u = \int_o^{Ld} \varepsilon_z dZ = \int_o^{Ld} 2\tau(L_d - Z)/E_f R dZ = \tau L_d 2/(E_f R) \tag{A5}$$

The debonding length can then be obtained from eqn (A5) as:

$$L_d = (E_f Ru/\tau)^{1/2} \tag{A6}$$

By inserting eqn (A6) into (A1), the tensile stress in the fiber between the crack faces can be expressed as a function of u as:

$$\sigma_1(u) = 2L_d\tau/R = (4E_f\tau u/R)^{1/2} \tag{A7}$$

which is eqn (5) in the text.

Appendix B

If L_{fd} is the maximum debonding length before fiber failure, and $2u_0$ is the maximum COD before fiber failure, then at the crack plane where $Z = O$:

$$\sigma_f(0) = 2\tau L_{df}/R \tag{B1}$$

Similarly, the stress in the fiber at the fiber position just before fiber failure is:

$$S = 2\tau(L_{fd} - L_p)/R \tag{B2}$$

with L_p the pull-out length of the fibers. Right before fiber failure, eqn (A7) becomes:

$$\sigma_f(u_o) = (4E_f\tau u_o/R)^{1/2} \tag{B3}$$

Combining eqns (B1) and (B2) gives:

$$S = \sigma(0)(L_{fd} - L_p)L_{fd} \tag{B4}$$

From eqns (B1)–(B4), it can be obtained that:

$$4(L_p\tau)^2/R^2 + 4\tau(L_pS - u_0E_f)/R + S^2 = 0 \tag{B5}$$

By solving eqn (B5) for τ, eqn (7) in the text can be obtained. By combining eqns (B2) and (7), (16) in the text can be obtained.